Hindawi
Journal of Nanomaterials
Volume 2019, Article ID 4658215, 9 pages
https://doi.org/10.1155/2019/4658215

Research Article

Graphene and MWCNT Printed Films: Preparation and RF Electrical Properties Study

Simone Quaranta,[1] Mauro Giorcelli,[2] and Patrizia Savi[3]

[1]*Department of Information, Electronics and Telecommunications Engineering (DIET), Sapienza University of Rome, Rome, Italy*
[2]*Department of Applied Science and Technology (DISAT), Politecnico di Torino, Torino, Italy*
[3]*Department of Electronics and Telecommunications (DET), Politecnico di Torino, Torino, Italy*

Correspondence should be addressed to Patrizia Savi; patrizia.savi@polito.it

Received 22 October 2018; Revised 24 January 2019; Accepted 7 February 2019; Published 18 April 2019

Academic Editor: Miguel A. Correa-Duarte

Carbon materials are well known for being a versatile class of materials able to transmit an electrical signal when used as fillers in composites. Among numerous carbon fillers, carbon nanotubes and graphene have been extensively investigated for the last thirty years. This paper compares graphene and carbon nanotube electrical (i.e., resistive and reactive) properties in the microwave range up to 3 GHz. The transmission and reflection parameters of both the microstrip transmission lines and patch antennas loaded with 33 wt.% of graphene and multiwalled carbon nanotubes (MWCNTs) were analyzed. Interestingly, for an identical composite matrix composition, different scattering parameters stemmed from the different morphology of the films, the diverse interactions between the graphene nanoplatelets, MWCNTs, and polymeric binders in conjunction with the intrinsic electrical characteristics of the two carbon materials.

1. Introduction

The incorporation of micro- and nanophase carbon particles in polymers has been a commonly employed technology to improve material performance since the early 1990s. The filler type and its concentration in polymer composites allow the material properties to be tuned [1, 2]. Among carbon fillers, carbon nanotubes (CNTs) and graphene have been the most commonly adopted in the last decade (see e.g., [3, 4]).

As far as CNTs are concerned, some recent examples of their application according to their electrical, mechanical, and thermal properties and their influence on the composite characteristics are reported in [5–8]. CNTs, with their tubular structure, could be considered as seamless cylinders formed by rolled-up graphene sheets with carbon atoms covalently bonded with each other through sp2 hybridization. Depending on the number of layers of the graphene sheets, they are further categorized into single-walled, double-walled, and multiwalled CNTs. Evaluating defectiveness and graphitization grade is an important way to classify the quality of CNTs.

Graphene, and in particular graphene nanoplatelets and their derivatives (i.e., reduced graphene oxide), is another interesting carbon material that has been studied in composites and compared to CNTs [9]. Graphene is the thinnest and lightest sp2 carbon nanomaterial, consisting of a one-atom-thick planar sheet of sp2-bonded carbon atoms in a honeycomb crystal lattice, and possesses extraordinary properties: excellent thermal and electrical conductivity, large surface area, fast heterogeneous electron transfer rates, and high mechanical strength. Monolayer graphene can be synthetized for particular applications, but in composites, where the quantities of materials are relevant, it is not possible to use monolayer graphene. In this case, graphene nanoplatelets are more appropriate. Also in this case, as for CNTs, defectiveness and graphitization grade could be used to classify the graphene quality and, as a consequence, its performance in composites.

Among the different investigations concerning carbon-based composites, a "niche" field is represented by thick films [10]. Their possible applications span from gas sensors and RFID [11, 12] to actuators and conductive

electrodes [13, 14] and microwave sensors [15]. Screen printing constitutes the most employed additive manufacturing technique for the deposition of thick films [16].

In this work, we report a comparison between MWCNT and graphene nanoplatelet screen-printed films. The two carbon materials and their films were morphologically and structurally investigated by Field Emission Scanning Electron Microscopy (FESEM) and Raman (level of defectiveness and graphitization). The scattering parameters (S_{11} and S_{12}) of the microstrip lines and of the inset-fed patch antennas properly loaded with a thick film were measured and the characteristics of the different films compared. The measured data were compared to the full-wave simulations of CST Microwave Studio.

2. Materials and Methods

2.1. Carbon Filler and Composite. MWCNTs were produced using combustion chemical vapor deposition by Nanothinx (Greece) and commercially labelled as NTX-1. Their nominal characteristics are external diameters 15-35 nm, internal diameters 3.5-12 nm, length ≥ 10 μm, surface area 200-250 m^2/g, and bulk density 0.16 g/cm^3.

The graphene nanoplatelets are produced by Nanoinnova (Spain) and commercially labelled C97. The manufacturer declared a surface area of ~45 m^2/g and a carbon content over 98.9 wt.% (EDS).

α-Terpineol (Sigma-Aldrich, b.p. 220°C), of Butvar 98 polyvinyl-butyral (PVB, molecular weight 40.000 −70.000 g/mol. determined by size exclusion chromatography, Sigma-Aldrich), polyvinyl-pyrrolidone (PVP, average molecular weight 360.000 g/mol., Sigma-Aldrich), and linoleic acid (≥99%, Sigma-Aldrich) were employed for the formulation of the organic vehicle of the screen printing paste.

2.2. Film Preparation. α-Terpineol-based screen printing pastes comprising a thermoplastic binder with two components (i.e., polar and nonpolar) additives and two different carbon fillers were prepared. 33 wt.% of MWCNT and graphene nanoplatelet particles were employed as conductive fillers in the final paste formulation. The organic vehicle was composed of 6.0 wt.% of Butvar (PVB), 1.7 wt.% of polyvinyl-pyrrolidone (PVB), and 3.1 wt.% of linoleic acid. PVB (nonpolar polymer) and PVP (polar polymer) constituted the binder part of the vehicle. Furthermore, PVB was also used as a thickener in order to improve the paste viscosity and enhance the thixotropic effect during printing. Because of the absence of any cross-linking agent (i.e., transition metal salts), the thermal curing of the linoleic acid was hindered. Thereby, the linoleic acid was just used as a wetting agent and dispersant additive to functionalize the carbon filler surface and prevent its agglomeration. All the paste components were presolubilized in anhydrous ethanol before being mixed and sonicated for 16 h by using a titanium ultrasonic horn. The ethanol was removed by evaporation under reduced pressure at 40°C. The pastes, containing the three different carbon fillers, were printed across a 3×3 mm^2 gap between a copper-etched microstrip onto an FR-4 substrate by means of a 230 mesh/inch polyester screen (see Figure 1). Film thicknesses of 30-40 μm were attained by repeating the printing procedure three times. A drying step between layer depositions was carried out at 125°C. The final thermal curing aimed at evaporating the solvent (i.e., α-terpineol) was performed in a muffle at 160°C for 3 hours.

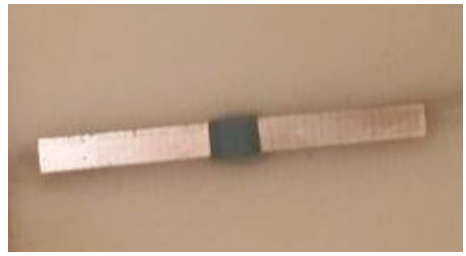

Figure 1: Examples of carbon film obtained using screen printing technique.

2.3. FESEM. In order to analyze the structure of the carbon particles and composite films, FESEM analysis was performed with a ZEISS SUPRATM 40 field emission scanning electron microscope.

2.4. Raman Characterization. Raman spectroscopy on MWCNTs and graphene nanoplatelets was performed using a Renshaw Ramascope MicroRaman, equipped with an argon green laser (excitation at 514.5 nm at 50 mW). Measurements were taken at different points for each carbon sample, with a 50x objective.

2.5. Microwave Film Characterization and Modeling. In order to compare the behavior of the films with MWCNTs and graphene, the films were printed across the gap of a microstrip line and the scattering parameters of the lines were measured with a Network Analyzer (Agilent E8361A). These lines were also modelled using a full-wave software (CST Microwave Studio) and the simulated results compared with the measurements.

3. Results and Discussion

3.1. FESEM Characterization. FESEM characterizations were performed on carbon materials and films. Some significant FESEM images for carbon materials are reported in Figure 2 while in Figure 3 are reported FESEM images of printed films.

MWCNTs appeared much entangled (see Figure 2(a)). Bundles of few microns in diameter are visible. When the magnification increases (Figures 2(b) and 2(c)), it is possible to appreciate the isolated MWCNTs with nominal tube diameters in the range 15-35 nm, as claimed by the producer.

Graphene is organized in nanoplatelets as reported in Figure 2(d) where platelets of few nanometers in thickness are formed by graphene layer. Increasing the magnification, it is possible to observe the flake structures as shown in Figure 2(e). At the very high magnification (800 KX, Figure 2(f)), transparent structure could be observed.

Figures 3(a)–3(c) show MWCNTs uniformly distributed into the polymer matrix. MWCNT diameters increased due

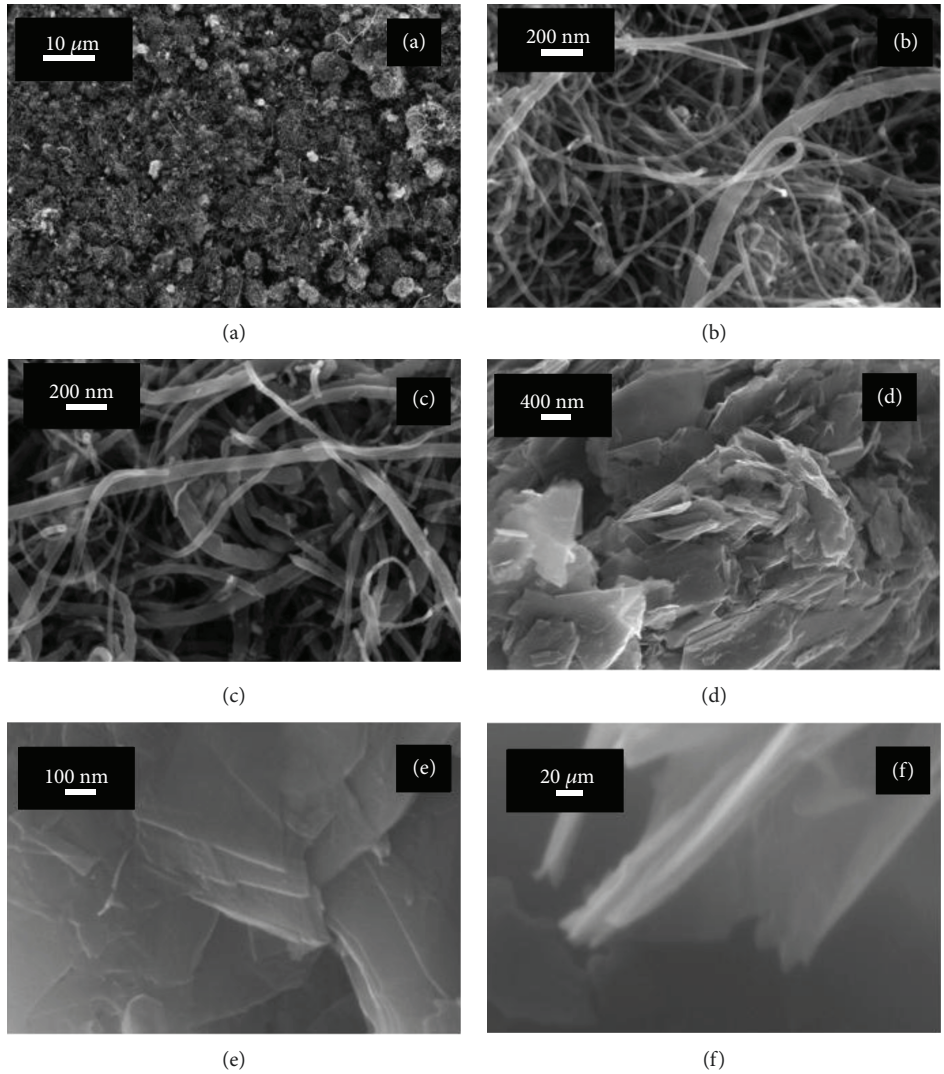

Figure 2: FESEM images of (a, b, c) MWCNTs and (d, e, f) graphene nanoplatelets.

to the coating layer comprising the PVP and PVB binders as shown in the inset of Figure 3(c). Figures 3(d)–3(f) show the morphological structure of film containing graphene nanoplatelets. In Figure 3(f), a disordered structure of graphene nanoplatelets could be observed. This is due to the PVP binder exerting a specific action during the dispersion of graphene nanoplatelets into the screen printing paste vehicle. Indeed, PVP high molecular mass together with its polar functional groups (the pyrrolidone ring) contributed to delaminate and deform (i.e., bending) the graphene layers resulting into a disordered structure composed of randomly arranged flakes (Figure 3(f)).

3.2. Raman Characterization. Raman analyses were performed on graphene nanoplatelets and MWCNTs. Their spectra are shown in Figure 4. In Raman signal on carbon materials, there are two main peaks: D and G peaks [17]. The D peak (breathing mode, A1g-band) is positioned in the 1300-1400 cm^{-1} range and it is related to the edge disorder in carbon structure. The G peak (tangential mode, E2g-band) is positioned in the 1550-1615 cm^{-1} range and corresponds to the stretching mode of sp2 bonds in the graphite plane. Second-order peaks could be observed in the range 2500-3500 cm^{-1}. These peaks represent the graphitization of the carbon material. In particular, the peak called 2D in this region is important in graphitic material [18]. Its asymmetric shape is the index of multilayer structure [19]. The graphitization of carbon material could be also appreciated observing the peak width that became important for the evaluation of graphitic material. The more the peak sharpness increases, the more the material is graphitized. The ratio between the intensity of D and G peaks (I_D/I_G) is used to evaluate the ratio between disordered and graphitized structures in the carbon material tested.

In our case, we evaluated the I_D/I_G ratio by fitting the D and G peaks with appropriated curves and calculating its area. This area takes into account peak intensity and its shape, with particular emphasis on its width. The fitting procedure performed on all the Raman spectra made it possible to calculate the I_D/I_G ratio and fill Table 1. Graphene nanoplatelet Raman spectra showed very sharp G peak and asymmetric 2D peak (shoulder on the left) that is the index of

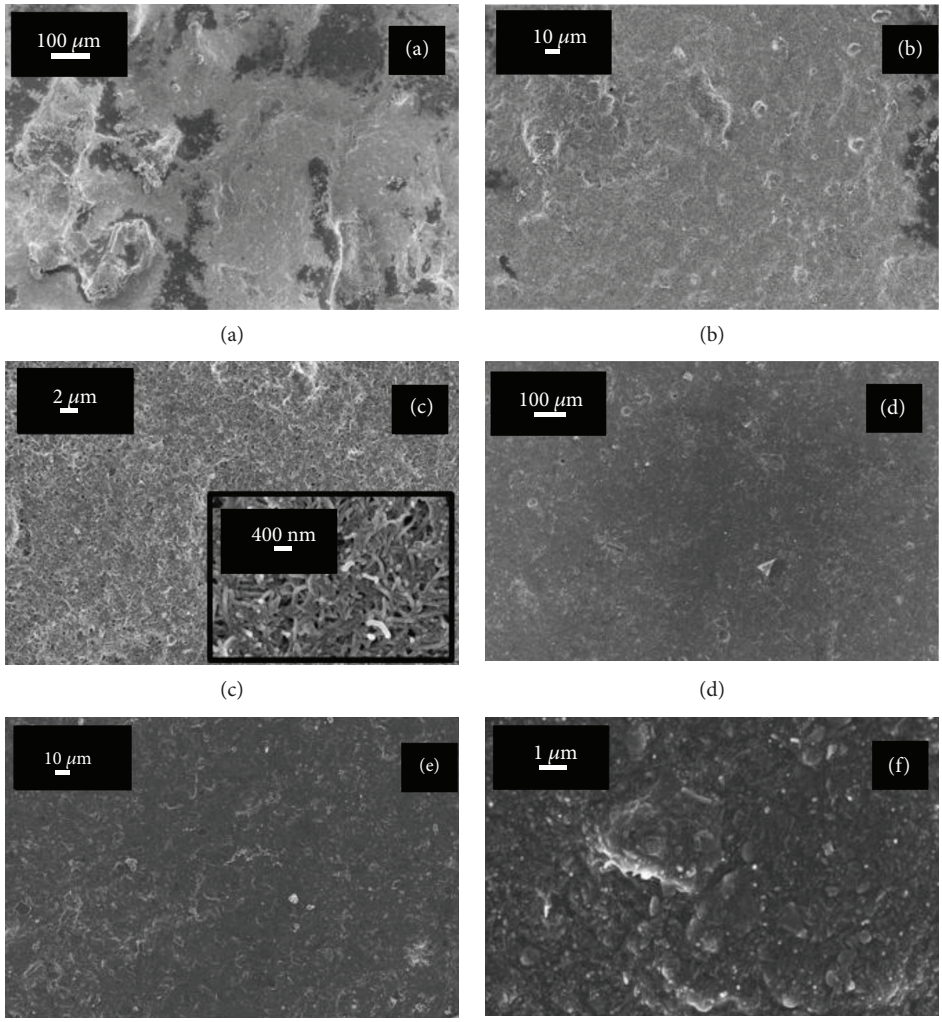

Figure 3: FESEM images of screen-printed films produced using as filler: (a, b, c) MWCNTs and (d, e, f) graphene nanoplatelets.

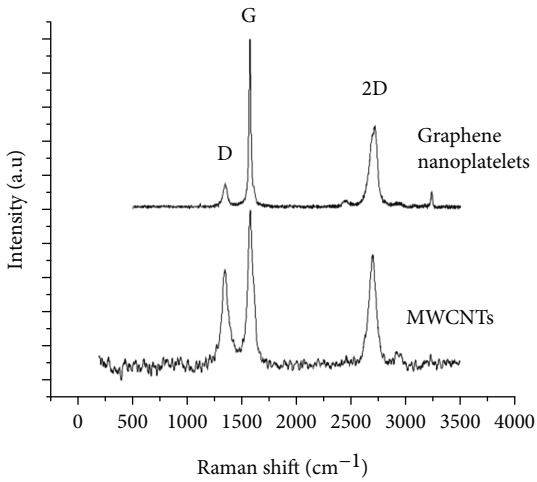

Figure 4: Raman spectra for MWCNTs and graphene nanoplatelets.

Table 1: I_D/I_G ratios for MWCNTs and graphene nanoplatelets.

Carbon material	I_D/I_G
MWCNTs	0.78
Graphene nanoplatelets	0.21

multilayer structures as expected. Graphene nanoplatelets reported the lowest I_D/I_G ratio. Graphitization grade influences the carbon material electrical properties [19].

3.3. Microwave Film Characterization. In order to understand the differences in the radiofrequency range between the MWCNT and graphene films, we considered a microstrip line (width 3 mm) printed on a FR-4 substrate (nominal dielectric constant 4.3, loss tangent 0.02, thickness 1.56 mm) with a centered gap (see Figure 5). A film of graphene of MWCNT of dimensions 3×3 mm was screen printed across the gap. The scattering parameters of the lines were measured after a standard 2-port calibration with a network analyzer.

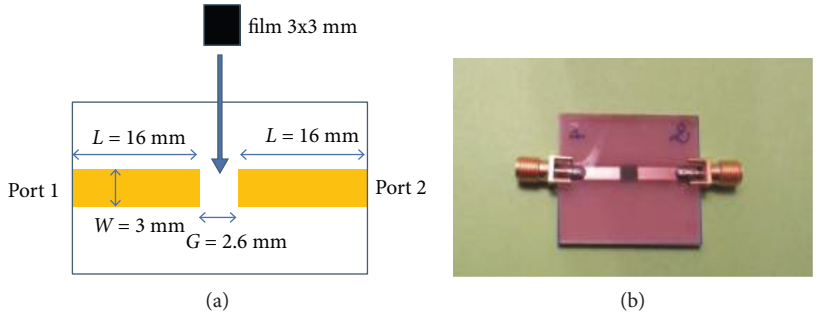

Figure 5: Sketch of the microstrip line with a centered gap (a). Realization of the line on a FR-4 substrate (b).

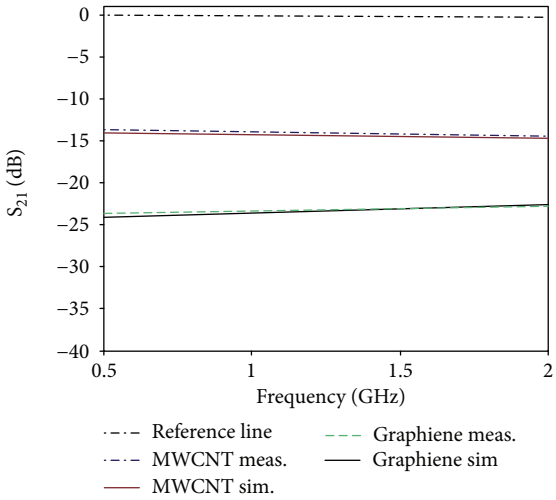

Figure 6: Transmission coefficient of microstrip lines loaded with MWCNT and graphene thick films (33 wt.%).

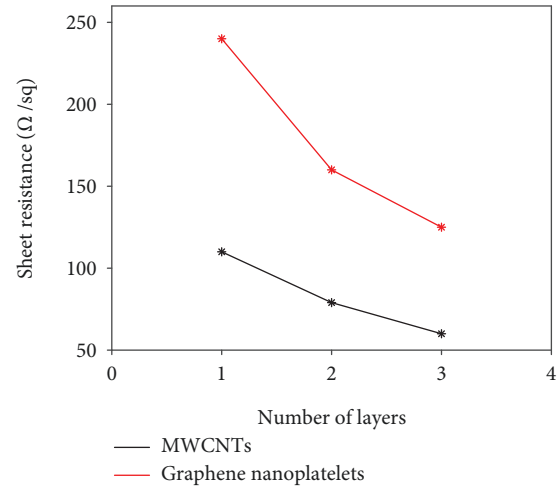

Figure 7: Sheet resistance (four-probe measurements) for different screen-printed layers of graphene and MWCNT composites cured at 160°C for 3 h.

Figure 6 displays the transmission coefficients (i.e., scattering parameter S_{21}) of the graphene- and MWCNT-loaded microstrip lines. Both samples were compared to the "reference" (i.e., no gap) copper microstrip line. Needless to say, the transmission coefficient of the two carbon materials is severely lower than the etched copper line one [20, 21]. Not surprisingly, etched copper conductive traces are largely conductive compared to screen-printed fillers. Indeed, the sheet resistance of conductive elements (i.e., MWCNTs or graphene) within a thick film is mainly determined by their level of interconnection [22]. Therefore, the relatively low curing temperature (160°C) used for the removal of the paste solvent is not sufficient to accomplish the sintering of the filler. Furthermore, bulk resistivity of MWCNTs (i.e., 1.6×10^{-5} Ωm for ballistic limit for a single CNT [20]) is three order of magnitude higher than the corresponding copper value. On the other hand, graphene's resistivity is comparable to the one of silver. However, such a behavior is ascribable to a single graphene layer [23]. Graphene thick films inevitably tend to resemble graphite resulting in lower electronic conductivity. In addition, the morphological characteristics of the composite materials must be taken into account in order to compare the electrical properties of the graphene and MWCNT films (see Figure 6). In fact, the large aspect ratio of MWCNTs [24] improves the level of electrical interconnectivity between nanostructures compared to the graphene nanoplatelets. In the same figure, the solid lines represent the simulated results obtained with CST Microwave Studio. In the case of graphene, the measured data were fitted considering a film about 60 S/m, whereas in the case of MWCNTs the specific conductivity turned out to be 180 S/m.

Besides, FESEM micrographs (Figures 1 and 2) show a discontinuous arrangement of the nanoplatelets and perhaps damage of the graphene structure (see Figure 2(f)). Thereby, the electron diffusion through the nanoplatelets may result hindered by the electrical resistance associated to the interface between the graphene planes. Moreover, while MWCNTs are coated by the polymeric matrix, the two binders (specially the PVP because of its higher molecular weight) interpose between the graphene planes causing the distortion of the structure and therefore a lower electronic conductivity. Figure 7 reports the sheet resistance data (measured in DC) of graphene and MWNCT films. Obviously, the sheet resistances of both composites decrease as the number of printed layers (thickness) increases. Nevertheless, the graphene film shows as much as twice the sheet of the MWCNT one. This outcome agrees with the behavior of the two films in the microwaves range. In fact, the simulated results (solid lines, Figure 6) obtained by modeling the film as a sheet resistance are $R = 1100$ Ohm/sq in the case of graphene and $R = 400$ Ohm/sq in the case of MWCNTs.

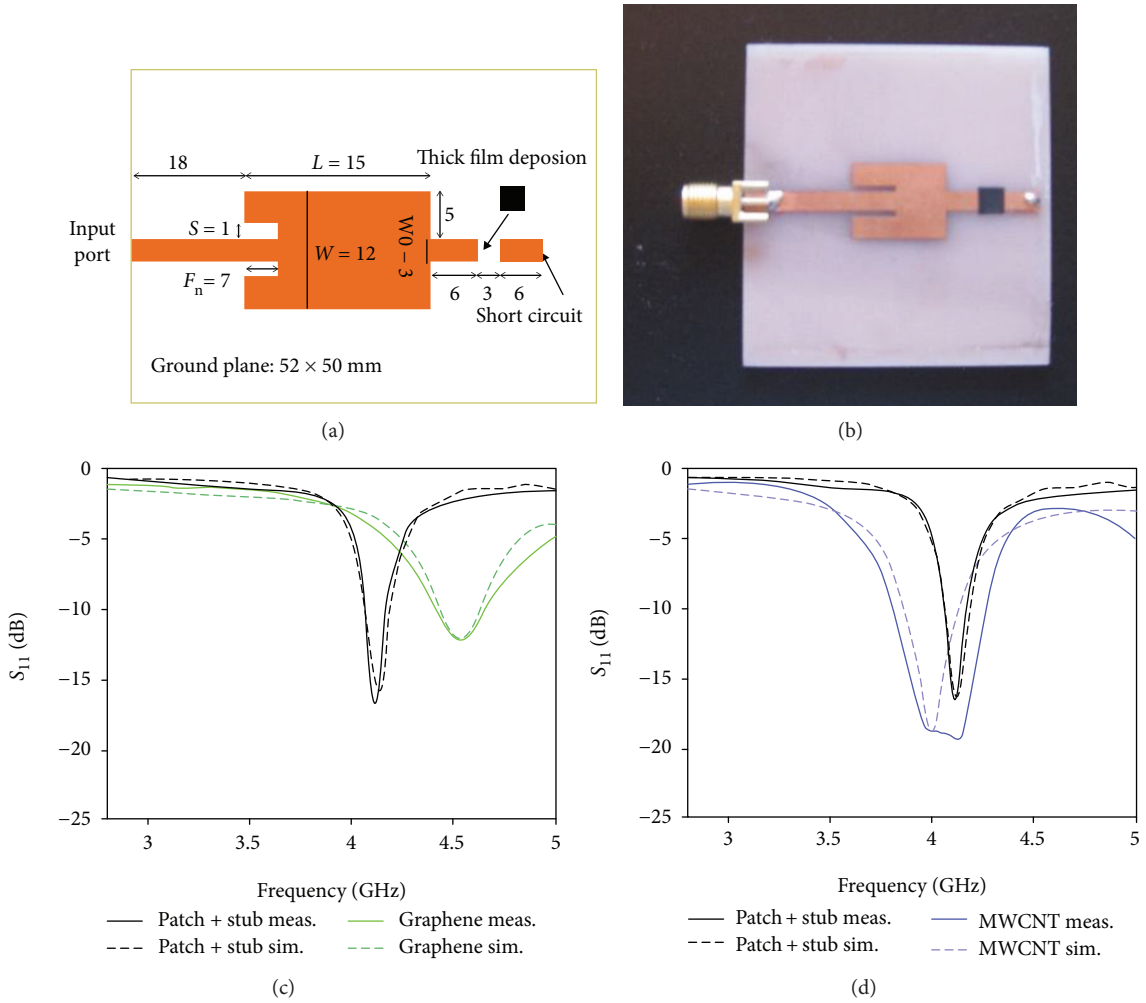

Figure 8: (a) Sketch of the antenna dimensions. (b) Picture of an antenna prototype. (c) Reflection coefficient of inset-fed patch antenna loaded with graphene films compared with the patch+stub configuration. (d) Reflection coefficient of inset-fed patch antenna loaded with MWCNT films compared with the patch+stub configuration.

3.4. An Example of Application: Inset-Fed Patch Antennas. An inset-fed microstrip patch antenna is designed to operate at 4.36 GHz (patch 15×12 mm^2, feed line width of 3 mm for 50 Ω impedance, see Figure 8). The feed inset and spacing (6 mm and 1 mm, respectively) are chosen to provide the best impedance match between the feed line and the patch. The original design was modified by adding a stub of length of 15 mm including a centered gap of 3 mm, as proposed in [25]. The antenna was fabricated on FR4 substrate (nominal dielectric constant of 4.3 and loss tangent of 0.02). A film of graphene or MWCNT, both 33 wt.% of size 3×3 mm^2 of three layers in thickness, was deposited across the gap.

The reflection coefficients of both antennas (loaded with MWCNTs and graphene nanoplatelets) were measured by using a network analyzer and contrasted with an etched antenna comprising only the copper patch and the 6 mm stub (see Figure 8). This latter device was considered the reference (resonant frequency 4.12 GHz). The antenna loaded with graphene film shows a resonant frequency of 4.5 GHz, while a wide band resonating around 4.05 GHz characterizes the MWCNT antenna. Therefore, the data seem to suggest an inductive frequency shift (toward higher frequencies) caused by the graphene and a capacitive (to the lower frequencies) brought about by MWCNTs with respect to the reference antenna. This behavior was also verified by means of full-wave simulations with CST Microwave Studio, 2018 (see Figure 8 dashed lines). The inset-fed microstrip antenna, the stubs, and the ground plane were modeled as copper with conductivity 5.8×10^7 S/m. The FR4 substrate was modeled by using a function describing the frequency dependence of the real part of permittivity and tan (δ). Although the Drude model may be used to simulate the microwave behavior of graphene flakes [26], it could not be applied to the present case because of the composite nature of the film. Indeed, the Drude model does not take into account the dielectric relaxation possibly associated to the polar binder. Therefore, the composite thick film scattering parameters were modeled through their surface impedance $Z = R + jX$ (Ohm/sq). In the case of MWCNT film, fitting between the measurements and the simulations was obtained considering $R = 100$ and $X = -550$, whereas in the case of graphene the values were $R = 1000$ and $X = +4000$. The graphene high R

compared to MWCNTs reflects the characteristics already shown in Figures 6 and 7. Nonetheless, R values attained by microwave simulation do not exactly correspond DC sheet resistance of the films because of the skin effect. Furthermore, the simulated X values (positive for graphene and negative for MWCNTs) agree with the inductive (i.e., MWCNTs) and capacitive (i.e., graphene) resonant frequency shifts reported in Figure 8.

However, such a different behavior cannot be explained neither in terms of kinetic inductance nor in terms of chemical capacitance. Indeed, the graphene kinetic inductance stemming from the motions of plasmos does not contribute to any impedance change unless the operative frequency of the antenna lies in the THz range [27, 28]. On the other hand, any contribution to the impedance due to the chemical capacitance (associated to the electronic density of states) of both carbon materials is not to be expected because of the high operative frequency [29].

Nevertheless, it is well known that dielectric properties of polymer-carbon material composites strongly depend on the electrical (i.e., conductivity), chemical (i.e., functional groups), geometrical (i.e., aspect ratio, specific surface area, and consequently percolation threshold), and morphological (i.e., dispersion into the matrix) properties of the filler [24, 30].

Hence, the different electronic density (i.e., band structure) of graphene nanoplatelets and MWCNTs can affect the antenna resonant frequency. Indeed, the rolling of a graphene sheet at a particular angle (i.e., chirality) results in a large variety of single-walled carbon nanotubes characterized by a distribution of electronic structures (i.e., metallic and semiconductor) [31–33]. Although MWCNTs are statistically metallic, their concentric structure comprised of interspaced folded graphene sheets inevitably generates an electronic density of state quite different compared to randomly distributed graphene flakes. Needless to say, such a difference affects the extension of the interaction between the carbon materials and the binder(s) at the graphene platelets (or MWCNTs)/polymer interface. In other words, since the two nanostructures possess two distinct electronic distribution, the effect of the van der Waals (intermolecular) forces (e.g., dipole-dipole, dipole-induced dipole, London dispersion forces, hydrogen bonds) [34, 35] regulating the filler-binder interaction may lead to different dielectric behaviors for the two cases [30]. These aspects can be particularly relevant for polar binders dielectrically relaxing in the microwave region like the PVP and PVP+PVB mixtures [35]. In addition, the interfacial electrical properties (i.e., surface impedance) of the two carbon are affected by the chemisorption, through the carboxylic-mediated covalent bond, of the linoleic acid used as dispersant in the paste formulation [36]. MWCNTs and graphene platelet band structures may differently impact on the -COO surface adsorption and therefore on the surface charge of the composite. For instance, it has been already reported [37, 38] that the wrinkling of graphene nanoplatelets (see Figure 3) and their surface treatment (i.e., with linoleic acid) can lower the dielectric permittivity of graphene. Furthermore, a high enough wt.% (over the percolation threshold) of graphene nanoplatelets distributed inside the polymeric medium can function as nanoscale electrostatic capacitors [39–42]. Therefore, the dielectric permittivity lowering (with respect to the gap dielectric that is the FR-4 and MWCNTs) can produce a reduction of the antenna capacitance, reflecting into an impedance increase and in turn causing the resonant frequency to shift to higher frequency. On the other hand, the large specific surface area of MWCNTs, and therefore the high interfacial polarization, may result into a slight shift of the resonant frequency toward lower frequency [30].

4. Conclusions

Two different films, containing different carbon materials at 33 wt.% (MWCNTs and graphene nanoplatelets), have been produced by screen printing technique. PVB and PVP were used as the binder to print tracks on FR4 substrates. The carbon materials were investigated from a morphological point of view and their graphitization grade was evaluated by Raman spectroscopy. The morphological and electrical characterizations of the carbon-based films were performed.

A detailed investigation of the composite morphology of the films by using FESEM revealed different arrangements of the two fillers across the film. Specifically, MWCNTs appeared to be uniformly covered with the binders without any relevant curling, while the graphene nanoplatelets, most likely because of the interaction of the more polar and heavier of the binders (PVP), were disorganized, partially disrupted and wrinkled. These characteristics also affected the electrical conductivity and radiofrequency scattering parameters. In particular, the improved electrical interconnectivity throughout the film of MWCNTs, stemming from their high aspect ratio, led to low sheet resistances (Rsh $\approx$ 60 Ω/sq in DC). On the contrary, the disarrayed graphene and curled nanoplatelets caused a lower level of electrical percolation across the composite slowing down the electron diffusion (Rsh $\approx$ 120 Ω/sq in DC). Consequently, the microwave transmission coefficient (S_{21}) of MWCNT thick films inserted into a microstrip transmission line was higher (around 10 dB) than that of their graphene counterpart. Moreover, the dielectric properties of the films turned out to be affected both by the different morphology of the two composites and by the various interactions at the polymer carbon filler interface. Indeed, the different electronic density of the two nanomaterials may impact on both the Van der Waals dipole forces (i.e., permanent and induced) and the chemical effect (i.e., chemisorption of linoleic acid) dictating the interaction between the filler, binder, and dispersant. These effects can account for the resonant frequency "inductive" shift (to higher frequencies) of the graphene-loaded antennas when compared to the MWCNT-loaded or merely copper-etched antennas. Indeed, as previously reported, the surface functionalization of graphene nanoplatelets (and steric interaction with polymers) causes a dielectric permittivity decrease, which is due to a surface impedance increase, and ultimately a shift in the resonant frequency of the return loss of the antenna. On the other hand, the high specific surface area of MWCNTs produced an extended interfacial polarization, avoiding a significant resonant frequency shift.

Data Availability

The data used to support the findings of this study are available from the corresponding author upon request.

Conflicts of Interest

The authors declare that there is no conflict of interest regarding the publication of this paper.

Acknowledgments

The authors would like to thank Ing. Salvatore Guastella for FESEM analysis; Nanothinx, Greece, for carbon nanotube supply; Massimo Rovere for Raman measurements and spectra fit; and Prof. Franco Maddaleno for the valuable comments.

References

[1] D. R. Paul and L. M. Robeson, "Polymer nanotechnology: nanocomposites," *Polymer*, vol. 49, no. 15, pp. 3187–3204, 2008.

[2] S. Kumar, R. Purohit, and M. M. Malik, "Properties and applications of polymer matrix nano composite materials," *Materials Today: Proceedings*, vol. 2, no. 4-5, pp. 3704–3711, 2015.

[3] U. K. Sur, "Graphene: a rising star on the horizon of materials science," *International Journal of Electrochemistry*, vol. 2012, Article ID 237689, 12 pages, 2012.

[4] V. Dhand, K. Y. Rhee, H. J. Kim, and D. H. Jung, "A comprehensive review of graphene nanocomposites: research status and trends," *Journal of Nanomaterials*, vol. 2013, Article ID 763953, 14 pages, 2013.

[5] T. McNally and P. Pötschke, Eds., *Polymer-Carbon Nanotube Composites*, Woodhead Publishing, 2011.

[6] Z. Han and A. Fina, "Thermal conductivity of carbon nanotubes and their polymer nanocomposites: a review," *Progress in Polymer Science*, vol. 36, no. 7, pp. 914–944, 2011.

[7] J. Li, "Multiwalled carbon nanotubes reinforced polypropylene composite material," *Journal of Nanomaterials*, vol. 2017, Article ID 2171356, 5 pages, 2017.

[8] J. Li, "Effect of multiwalled carbon nanotubes (MWNT) on the properties of high impact polystyrene (HIPS)," *Journal of Nanomaterials*, vol. 2018, Article ID 8305721, 5 pages, 2018.

[9] X. Sun, H. Sun, H. Li, and H. Peng, "Developing polymer composite materials: carbon nanotubes or graphene?," *Advanced Materials*, vol. 25, no. 37, pp. 5153–5176, 2013.

[10] E. Shi, H. Li, L. Yang et al., "Carbon nanotube network embroidered graphene films for monolithic all-carbon electronics," *Advanced Materials*, vol. 27, no. 4, pp. 682–688, 2015.

[11] T. Zhang, S. Mubeen, E. Bekyarova et al., "Poly(m-aminobenzene sulfonic acid) functionalized single-walled carbon nanotubes based gas sensor," *Nanotechnology*, vol. 18, no. 16, pp. 165504–165509, 2007.

[12] N. C. Karmakar, E. M. Amin, and J. K. Saha, *Chipless RFID Sensors*, John Wiley & Sons, Inc, 1st edition, 2016.

[13] X. Zang, Q. Zhou, J. Chang, Y. Liu, and L. Lin, "Graphene and carbon nanotube (CNT) in MEMS/NEMS applications," *Microelectronic Engineering*, vol. 132, pp. 192–206, 2015.

[14] J. Liang, X. Chen, M. Zhang, H. Zhang, D. Zhang, and W. Pang, "An RF-MEMS-resonator-driven graphene transistor," in *2018 IEEE Micro Electro Mechanical Systems (MEMS)*, pp. 771–774, Belfast, UK, 2018.

[15] L. Su, J. Mata-Contreras, P. Vélez, and F. Martín, "A review of sensing strategies for microwave sensors based on metamaterial-inspired resonators: dielectric characterization, displacement, and angular velocity measurements for health diagnosis, telecommunication, and space applications," *International Journal of Antennas and Propagation*, vol. 2017, Article ID 5619728, 13 pages, 2017.

[16] S. Quaranta, M. Miscuglio, A. Bayat, and P. Savi, "Morphological and radio frequency characterization of graphene composite films," *C-Journal of Carbon Research*, vol. 4, no. 2, pp. 1–12, 2018.

[17] A. C. Ferrari and D. M. Basko, "Raman spectroscopy as a versatile tool for studying the properties of graphene," *Nature Nanotechnology*, vol. 8, pp. 235–246, 2013.

[18] D. Mattia, M. P. Rossi, B. M. Kim, G. Korneva, H. H. Bau, and Y. Gogotsi, "Effect of graphitization on the wettability and electrical conductivity of CVD-carbon nanotubes and films," *The Journal of Physical Chemistry B*, vol. 110, pp. 9850–9855, 2006.

[19] C. F. Coombs Jr., Ed., *Printed Circuits Handbook*, McGraw-Hill, 6th edition, 2006.

[20] A. Salleo and W. S. Wong, Eds., *Flexible Electronics. Materials and Applications*, Springer, 1st edition, 2009.

[21] K. Gilleo, *Polymer Thick Film: Today's Emerging Technology for a Clean Environment Tomorrow*, Spinger, 1st edition, 1995.

[22] Y. Kim, B. Lee, S. Yang, I. Byun, I. Jeong, and S. M. Cho, "Use of copper ink for fabricating conductive electrodes and RFID antenna tags by screen printing," *Current Applied Physics*, vol. 12, no. 2, pp. 473–478, 2012.

[23] A. H. Castro Neto, F. Guinea, N. M. R. Peres, K. S. Novoselov, and A. K. Geim, "The electronic properties of graphene," *Reviews of Modern Physics*, vol. 81, no. 1, pp. 109–162, 2009.

[24] M. Giorcelli, P. Savi, M. Yasir, M. Miscuglio, M. H. Yahya, and A. Tagliaferro, "Investigation of epoxy resin/multiwalled carbon nanotube nanocomposite behavior at low frequency," *Journal of Materials Research*, vol. 30, no. 1, pp. 101–107, 2015.

[25] K. Naishadham, "An investigation on the tuning of a microstrip patch antenna using carbon nanotube thin films," in *2014 IEEE Antennas and Propagation Society International Symposium (APSURSI)*, pp. 900-901, Memphis, TN, USA, 2014.

[26] S. Bellucci, A. Maffucci, S. Maksimenko et al., "Electrical permittivity and conductivity of a graphene nanoplatelet contact in the microwave range," *Materials*, vol. 11, no. 12, p. 2519, 2018.

[27] F. Rana, "Graphene terahertz plasmon oscillators," *IEEE Transactions on Nanotechnology*, vol. 7, no. 1, pp. 91–99, 2008.

[28] T. L. Zinenko, A. Matsushima, and A. I. Nosich, "Surface-plasmon, grating-mode, and slab-mode resonances in the H- and E-polarized THz wave scattering by a graphene strip grating embedded into a dielectric slab," *IEEE Journal of Selected Topics in Quantum Electronics*, vol. 23, no. 4, pp. 1–9, 2017.

[29] J. Xia, F. Chen, J. Li, and N. Tao, "Measurement of the quantum capacitance of graphene," *Nature Nanotechnology*, vol. 4, pp. 505–509, 2009.

[30] A. A. Khurram, S. A. Rakha, P. Zhou, M. Shafi, and A. Munir, "Correlation of electrical conductivity, dielectric properties,

microwave absorption, and matrix properties of composites filled with graphene nanoplatelets and carbon nanotubes," *Journal of Applied Physics*, vol. 118, no. 4, article 044105, 2015.

[31] V. L. Davis, S. Quaranta, C. Cavallo, A. Latini, and F. Gaspari, "Effect of single-chirality single-walled carbon nanotubes in dye sensitized solar cells photoanodes," *Solar Energy Materials and Solar Cells*, vol. 167, pp. 162–172, 2017.

[32] H. Liu, T. Tanaka, Y. Urabe, and H. Kataura, "High-efficiency single-chirality separation of carbon nanotubes using temperature-controlled gel chromatography," *Nano Letters*, vol. 13, no. 5, pp. 1996–2003, 2013.

[33] R. M. Jain, M. Ben-Naim, M. P. Landry, and M. S. Strano, "Competitive binding in mixed surfactant systems for single-walled carbon nanotube separation," *The Journal of Physical Chemistry C*, vol. 119, no. 39, pp. 22737–22745, 2015.

[34] S. A. Ntim, O. Sae-Khow, F. A. Witzmann, and S. Mitra, "Effects of polymer wrapping and covalent functionalization on the stability of MWCNT in aqueous dispersions," *Journal of Colloid and Interface Science*, vol. 355, no. 2, pp. 383–388, 2011.

[35] S. C. Ray, "Comparison of electronic structure and magnetic properties of few layer graphene and multiwall carbon nanotubes," *Advances in Materials Science and Engineering*, vol. 2016, Article ID 7362131, 7 pages, 2016.

[36] A. Rawat, H. K. Mahavar, A. Tanwar, and P. J. Singh, "Dielectric relaxation studies of polyvinylpyrrolidone (PVP) and polyvinylbutyral (PVB) in benzene solutions at microwave frequency," *Indian Journal of Pure & Applied Physics*, vol. 52, no. 9, pp. 632–636, 2014.

[37] Y. B. Yi and E. Tawerghi, "Geometric percolation thresholds of interpenetrating plates in three-dimensional space," *Physical Review E*, vol. 79, article 041134, 2009.

[38] J. R. Potts, D. R. Dreyer, C. W. Bielawski, and R. S. Ruoff, "Graphenebased polymer nanocomposites," *Polymer*, vol. 52, pp. 5–25, 2011.

[39] L. Pierantoni, D. Mencarelli, M. Bozzi et al., "Broadband microwave attenuator based on few layer graphene flakes," *IEEE Transactions on Microwave Theory and Techniques*, vol. 63, pp. 2491–2497, 2015.

[40] P. Savi, K. Naishadham, A. Bayat, M. Giorcelli, and S. Quaranta, "Multi-walled carbon nanotube thin film loading for tuning microstrip patch antennas," in *2016 10th European Conference on Antennas and Propagation (EuCAP)*, pp. 1–3, Davos, Switzerland, 2016.

[41] P. Savi, K. Naishadham, S. Quaranta, M. Giorcelli, and A. Bayat, "Microwave characterization of graphene films for sensor applications," in *2017 IEEE International Instrumentation and Measurement Technology Conference (I2MTC)*, pp. 1–5, Torino, Italy, May 2017.

[42] M. Yasir, P. Savi, S. Bistarelli et al., "A planar antenna with voltage-controlled frequency tuning based on few-layer graphene," *IEEE Antennas and Wireless Propagation Letters*, vol. 16, pp. 2380–2383, 2017.